

NUMERICAL SIMULATION OF GRATING STRUCTURES INCORPORATING TWO-DIMENSIONAL MATERIALS: A HIGH-ORDER PERTURBATION OF SURFACES FRAMEWORK*

DAVID P. NICHOLLS[†]

Abstract. The plasmonics of two-dimensional materials, such as graphene, has become an important field of study for devices operating in the terahertz to midinfrared regime where such phenomena are supported. The semimetallic character of these materials permits electrostatic biasing which allows one to tune their electrical properties, unlike the noble metals (e.g., gold, silver) which also support plasmons. In the literature there are two principal approaches to modeling two-dimensional materials: With a thin layer of finite thickness featuring an effective permittivity, or with a surface current. We follow this latter approach to not only derive governing equations which are valid in the case of curved interfaces, but also reformulate these volumetric equations in terms of surface quantities using Dirichlet–Neumann operators. Such operators have been used extensively in the numerical simulation of electromagnetics problems, and we use them to restate the governing equations at layer interfaces. Beyond this, we show that these surface equations can be numerically simulated in an efficient, stable, and accurate fashion using a High-Order Perturbation of Surfaces methodology. We present detailed numerical results which not only validate our simulation using the Method of Manufactured Solutions and by comparison to results in the literature, but also describe Surface Plasmon Resonances at the “wavy” (corrugated) interface of a dielectric-graphene-dielectric structure.

Key words. high-order perturbation of surfaces methods, two-dimensional materials, graphene, high-order spectral methods, Helmholtz equation, diffraction gratings

AMS subject classifications. 78A45, 65N35, 78B22, 35J05, 41A58

DOI. 10.1137/17M1123481

1. Introduction. In the past decade the fields of plasmonics and photonics have been transformed with the introduction of “two-dimensional materials” into photonic devices. These single atom thick layered materials have remarkable mechanical, chemical, and electronic properties, and while several materials, such as black phosphorous [35] and hexagonal Boron Nitride (hBN) [33], have shown promise in practice, the most well-studied is graphene [25, 23, 22, 24, 58]. Graphene is a single layer of carbon atoms in a honeycomb lattice which was first isolated experimentally in 2004 [59] resulting in the 2010 Nobel Prize in Physics to Geim [24] and Novoselov [58]. The literature on the manufacture, modeling, and commercialization of graphene based devices is in the thousands [16] and up-to-date survey papers are difficult to identify (see the references above up to 2011). As further evidence of this, note that *Nature* maintains a specific web page for the latest publications in the field [1].

Graphene plasmonics has become an important field of study for devices operating in the terahertz to midinfrared regime [34] where such phenomena are supported. A vast number of applications for these materials are being found in communications, military capabilities, medical sciences, and biological sensing [68, 21, 66]. Graphene’s semimetallic character permits electrostatic biasing which allows one to tune its elec-

*Received by the editors March 30, 2017; accepted for publication (in revised form) September 26, 2017; published electronically January 2, 2018.

<http://www.siam.org/journals/siap/78-1/M112348.html>

Funding: This author’s work was supported by the National Science Foundation through grant DMS-1522548.

[†]Department of Mathematics, Statistics, and Computer Science, University of Illinois at Chicago, Chicago, IL 60607 (davidn@uic.edu).

trical properties, unlike the noble metals (e.g., gold, silver) which also support plasmons. With this in mind it is clear why graphene and other two-dimensional materials have garnered so much attention.

While extensive work has been conducted by the scientific and engineering communities on devices containing graphene, black phosphorous, and hBN, little has been done in the applied mathematics literature. However, we do point out the recent work of Auditore et al. [4], and Angelis et al. [2] which are not only focused on two important and interesting applications, but are also mathematically careful.

To place our current contribution in proper context, we note that in the literature there are two principal approaches to modeling two-dimensional materials: With a thin layer of finite thickness (perhaps only a few Angstroms) featuring an effective permittivity, or with a surface current. This latter approach is used in [4, 2] and we follow their lead in not only this, but also a careful and rigorous approach. In particular, we derive governing equations which are valid in the case of *curved* interfaces. Furthermore, we reformulate these volumetric equations in terms of surface quantities using Dirichlet–Neumann Operators (DNOs) which map Dirichlet data to Neumann data. Such operators have been used extensively in the numerical simulation of electromagnetics problems, both for the enforcement of far-field conditions transparently [27, 32, 17, 6, 18, 7, 26, 48, 28] and the restatement of the governing equation at layer interfaces [45, 38, 49, 47]. We follow this latter approach in restating the governing equations with surface currents in terms of DNOs.

Beyond this, we show that these surface equations can be numerically simulated in an efficient, stable, and accurate fashion using a High-Order Perturbation of Surfaces (HOPS) methodology. The latter is required as the relevant DNOs are highly nontrivial to compute for a *corrugated* interface, but there are many options including Bruno and Reitich’s Method of Field Expansions (FE) [10, 11, 12], the Method of Operator Expansions (OE) due to Milder [39, 40, 41, 42], and the Transformed Field Expansions (TFE) devised by Nicholls and Reitich [51, 54, 55]. Among these highly accurate and efficient methods, we focus upon the extremely rapid FE approach and the stabilized TFE method. We refer the interested reader to [51, 52, 54, 55, 69] for an extensive set of detailed computations which compare and contrast the behavior of these three algorithms.

The rest of the paper is organized as follows: In section 2 we discuss our model of a two-dimensional material between two dielectrics (though nothing in the formulation prevents either being a metal), specializing to two-dimensional problems in section 2.1, discussing the modeling of the two-dimensional material in section 2.2, and describing the equations for Transverse Electric (TE) and Transverse Magnetic (TM) polarizations in sections 2.3 and 2.4, respectively. In section 3 we outline our surface formulation of these equations, with details for the TE and TM equations in sections 3.1 and 3.2, respectively. We present the conditions for a Surface Plasmon Resonance (SPR) in these configurations in section 4. In section 5 we define the DNOs required for our surface formulation, and in sections 5.1 and 5.2 we discuss the FE and TFE methods for their computation. With these we describe our full HOPS methodology in section 6. To conclude, we present our numerical results in section 7, with validation by the Method of Manufactured Solutions in section 7.1 and by comparison with results in the literature in section 7.2. We present new results on SPRs induced at a “wavy” (corrugated) interface of a dielectric-graphene-dielectric structure in section 7.3. There are three appendices which discuss the derivation of Helmholtz equations in our models (Appendix A), the details of our surface conductivity model of graphene (Appendix B), and a vanishing layer thickness approach to

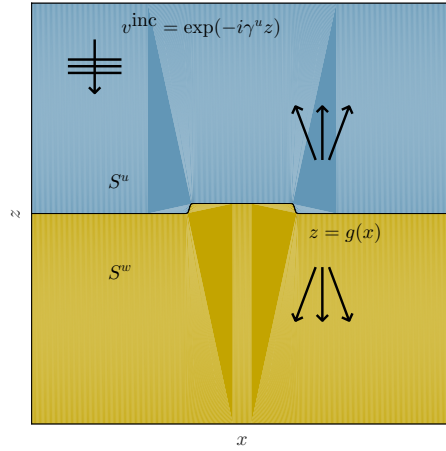


FIG. 1. Plot of two-layer structure with periodic interface.

modeling two-dimensional materials which validates our models in sections 3.1 and 3.2 (Appendix C).

2. The model. The configuration we consider is depicted in Figure 1: A doubly layered medium with interface specified by the doubly periodic grating shape

$$(2.1) \quad z = g(x, y), \quad g(x + d_x, y + d_y) = g(x, y),$$

giving two domains

$$(2.2) \quad S^u = \{z > g(x, y)\}, \quad S^w = \{z < g(x, y)\},$$

with permittivities $\{\epsilon^{(u)}, \epsilon^{(w)}\}$ and indices of refraction $\{n^{(u)}, n^{(w)}\}$, respectively. The two-dimensional material is modeled by a vanishingly thin medium at $z = g(x, y)$. The structure is illuminated from above with monochromatic plane-wave radiation of frequency ω and wavenumber $k^{(u)} = n^{(u)}\omega/c_0 = \omega/c^{(u)}$ (c_0 is the speed of light). The forms of these are

$$\mathbf{E}^i = \mathbf{A}e^{i\alpha x + i\beta y - i\gamma^{(u)}z}, \quad \mathbf{H}^i = \mathbf{B}e^{i\alpha x + i\beta y - i\gamma^{(u)}z},$$

where $\alpha^2 + \beta^2 + (\gamma^{(u)})^2 = (k^{(u)})^2$ in order to be a solution. The reduced (total) electric and magnetic fields satisfy the *time-harmonic* Maxwell equations [60, 71]

$$(2.3a) \quad \text{curl}[\mathbf{E}] = i\omega\mu_0\mathbf{H},$$

$$(2.3b) \quad \text{curl}[\mathbf{H}] = -i\omega\epsilon_0\epsilon\mathbf{E},$$

$$(2.3c) \quad \text{div}[\mathbf{E}] = 0,$$

$$(2.3d) \quad \text{div}[\mathbf{H}] = 0,$$

where

$$\epsilon := \epsilon' + i\frac{\sigma}{\omega\epsilon_0},$$

ϵ' is the relative permittivity, and σ is the (bulk) conductivity. The incident radiation generates reflected and transmitted fields ($\{\mathbf{E}^{(u)}, \mathbf{H}^{(u)}\}$ and $\{\mathbf{E}^{(w)}, \mathbf{H}^{(w)}\}$),

respectively) so that

$$\mathbf{E} = \begin{cases} \mathbf{E}^{(\mathbf{u})} + \mathbf{E}^{\mathbf{i}}, & z > g(x, y), \\ \mathbf{E}^{(\mathbf{w})}, & z < g(x, y), \end{cases} \quad \mathbf{H} = \begin{cases} \mathbf{H}^{(\mathbf{u})} + \mathbf{H}^{\mathbf{i}}, & z > g(x, y), \\ \mathbf{H}^{(\mathbf{w})}, & z < g(x, y). \end{cases}$$

Regarding boundary conditions we demand quasiperiodicity:

$$\mathbf{E}(x+d_x, y+d_y, z) = e^{i\alpha d_x + i\beta d_y} \mathbf{E}(x, y, z), \quad \mathbf{H}(x+d_x, y+d_y, z) = e^{i\alpha d_x + i\beta d_y} \mathbf{H}(x, y, z),$$

and that the fields be “outgoing.” Finally, at the material interface with normal vector \mathbf{N} (not necessarily normalized), we enforce the continuity of the tangential components of the electric field

$$\frac{\mathbf{N}}{|\mathbf{N}|} \times \mathbf{E} = 0,$$

which implies that

$$(2.4) \quad \mathbf{N} \times [\mathbf{E}^{(\mathbf{u})} - \mathbf{E}^{(\mathbf{w})}] = -\mathbf{N} \times \mathbf{E}^{\mathbf{i}},$$

while noting that the jumps in the tangential components of the magnetic field are given by the surface current, \mathbf{j}_s ,

$$\frac{\mathbf{N}}{|\mathbf{N}|} \times \mathbf{H} = \mathbf{j}_s,$$

which delivers

$$(2.5) \quad \mathbf{N} \times [\mathbf{H}^{(\mathbf{u})} - \mathbf{H}^{(\mathbf{w})}] = -\mathbf{N} \times \mathbf{H}^{\mathbf{i}} + |\mathbf{N}| \mathbf{j}_s.$$

In many situations this surface current is set to zero; however, we follow [4, 2] and use it as a device to simulate the presence of a two-dimensional material.

2.1. Two-dimensional periodic gratings. We now assume that the grating shape is y -invariant and d -periodic in x so that

$$z = g(x), \quad g(x+d) = g(x),$$

giving rise to a normal

$$\mathbf{N} = (-\partial_x g \quad 0 \quad 1)^T$$

and (longitudinal and transverse) tangents

$$\mathbf{T}_\ell = (1 \quad 0 \quad \partial_x g)^T, \quad \mathbf{T}_t = (0 \quad 1 \quad 0)^T.$$

We also align the incident radiation with the grooves of the grating. For instance, for TE polarization we have

$$\mathbf{E}^{\mathbf{i}} = \mathbf{A} e^{i\alpha x - i\gamma^u z}, \quad \mathbf{A} = (0 \quad A \quad 0)^T,$$

while for TM polarization we choose

$$\mathbf{H}^{\mathbf{i}} = \mathbf{B} e^{i\alpha x - i\gamma^u z}, \quad \mathbf{B} = (0 \quad B \quad 0)^T.$$

2.2. Surface current model of the two-dimensional material. At this point we turn to the question of incorporating the two-dimensional material into our model and, following the work of many others (e.g., [4, 2]), use the surface current $\sigma^{(g)}$ for this purpose. For this we use Ohm's Law, $\mathbf{J} = \sigma^{(g)}\mathbf{E}$, and take a *tangential* surface component

$$\mathbf{j}_s = \sigma^{(g)} \left(\frac{\mathbf{E}^{(w)} \cdot \mathbf{T}}{\mathbf{T} \cdot \mathbf{T}} \right) \mathbf{T},$$

where \mathbf{j}_s is measured in Amperes per meter and $\sigma^{(g)}$ is the surface conductivity measured in Siemens. In this equation we use a tangential component of the electric field which, due to tangential continuity (cf. (2.4)), equals both

$$(\mathbf{E}^{(u)} + \mathbf{E}^i) \cdot \mathbf{T} \quad \text{and} \quad \mathbf{E}^{(w)} \cdot \mathbf{T}.$$

We choose the latter as it is more convenient for our formulation.

2.3. Transverse electric (TE) polarization. In TE polarization we seek solutions for which the *electric* field has only a *transverse* component

$$\mathbf{E}(x, z) = (0 \quad v(x, z) \quad 0)^T = v(x, z)\mathbf{T}_t.$$

It is a straightforward computation (see Appendix A) to realize that, in the bulk, v must satisfy the Helmholtz equation

$$\Delta v + \epsilon k_0^2 v = 0,$$

where $k_0^2 = \omega^2 \epsilon_0 \mu_0$.

Regarding boundary conditions we begin by noting that, since $\mathbf{N} \times \mathbf{T}_t = -\mathbf{T}_\ell$,

$$\mathbf{N} \times \mathbf{E} = (-v)\mathbf{T}_\ell, \quad \mathbf{N} \times \mathbf{H} = \left(-\frac{1}{i\omega\mu_0} \partial_N v \right) \mathbf{T}_t.$$

Now, defining u , u^i , and w by the decomposition

$$v(x, z) = \begin{cases} u(x, z) + u^i(x, z), & z > g(x), \\ w(x, z), & z < g(x), \end{cases}$$

we begin by enforcing the continuity of the tangential component of the electric field at the interface $z = g(x)$, (2.4),

$$0 = \mathbf{N} \times \mathbf{E} = (-v)\mathbf{T}_\ell \quad \text{at } z = g(x),$$

which implies $u + u^i - w = 0$ or

$$u - w = -u^i \quad \text{at } z = g(x).$$

Next, we enforce the jump in a tangential component of the magnetic field (2.5). As the tangential component of $\mathbf{N} \times \mathbf{H}$ is in the transverse tangential direction, \mathbf{T}_t , we choose

$$\frac{\mathbf{E}^{(w)} \cdot \mathbf{T}_t}{\mathbf{T}_t \cdot \mathbf{T}_t} = w.$$

Thus we have

$$|\mathbf{N}| \sigma^{(g)} w \mathbf{T}_t = |\mathbf{N}| \sigma^{(g)} \left(\frac{\mathbf{E}^{(w)} \cdot \mathbf{T}_t}{\mathbf{T}_t \cdot \mathbf{T}_t} \right) \mathbf{T}_t = |\mathbf{N}| \mathbf{j}_s = \mathbf{N} \times \mathbf{H} = \left(-\frac{1}{i\omega\mu_0} \partial_N v \right) \mathbf{T}_t,$$

and we find

$$\partial_N u - \left\{ \partial_N - |\mathbf{N}| (i\omega\mu_0) \sigma^{(g)} \right\} w = -\partial_N u^i, \quad \text{at } z = g(x).$$

Considering a dimensionless surface current, $\hat{\sigma}^{(g)} = \sigma^{(g)} / (\epsilon_0 c_0)$, and using this and the fact that $\omega = c_0 k_0$, this equation simplifies to

$$\partial_N u - \left\{ \partial_N - |\mathbf{N}| \rho \right\} w = -\partial_N u^i \quad \text{at } z = g(x),$$

where

$$\rho = \rho(\omega) := i\omega\mu_0 \sigma^{(g)}(\omega) = ik_0 \hat{\sigma}^{(g)}.$$

We gather these results and state that we seek *quasiperiodic, outgoing* solutions of

$$(2.6a) \quad \Delta u + \epsilon^{(u)} k_0^2 u = 0, \quad z > g(x),$$

$$(2.6b) \quad \Delta w + \epsilon^{(w)} k_0^2 w = 0, \quad z < g(x),$$

$$(2.6c) \quad u - w = \zeta \quad \text{at } z = g(x),$$

$$(2.6d) \quad \partial_N u - \left\{ \partial_N - |\mathbf{N}| \rho \right\} w = \psi(x) \quad \text{at } z = g(x),$$

where

$$(2.6e) \quad \zeta(x) := -[u^i]_{z=g(x)}, \quad \psi(x) := -[\partial_N u^i]_{z=g(x)}.$$

2.4. Transverse magnetic (TM) polarization. In TM polarization we look for solutions for which the *magnetic* field has only a *transverse* component

$$\mathbf{H}(x, z) = (0 \quad v(x, z) \quad 0)^T = v(x, z) \mathbf{T}_t.$$

As before, an elementary calculation (see Appendix A) shows that v satisfies the Helmholtz equation

$$\operatorname{div} \left[\frac{1}{\epsilon} \nabla v \right] + k_0^2 v = 0.$$

Regarding boundary conditions we begin by noting that

$$\mathbf{N} \times \mathbf{H} = (-v) \mathbf{T}_\ell, \quad \mathbf{N} \times \mathbf{E} = \left(\frac{1}{i\omega\epsilon_0\epsilon} \partial_N v \right) \mathbf{T}_t.$$

Again, defining u , u^i , and w by the decomposition

$$v(x, z) = \begin{cases} u(x, z) + u^i(x, z), & z > g(x), \\ w(x, z), & z < g(x), \end{cases}$$

we begin by enforcing the continuity of the tangential component of the electric field at the interface $z = g(x)$, (2.4),

$$0 = \mathbf{N} \times \mathbf{E} = \left(\frac{1}{i\omega\epsilon_0\epsilon} \partial_N v \right) \mathbf{T}_t \quad \text{at } z = g(x),$$

which implies $(1/\epsilon^{(u)})\partial_N u + (1/\epsilon^{(w)})\partial_N u^i - (1/\epsilon^{(w)})\partial_N w = 0$ or

$$\partial_N u - \tau^2 \partial_N w = -\partial_N u^i \quad \text{at } z = g(x),$$

where

$$\tau^2 := \frac{\epsilon^{(u)}}{\epsilon^{(w)}}.$$

Once again, we enforce the jump in a tangential component of the magnetic field (2.5). As the tangential component of $\mathbf{N} \times \mathbf{H}$ is in the longitudinal tangential direction, \mathbf{T}_ℓ , we need

$$\frac{\mathbf{E}^{(w)} \cdot \mathbf{T}_\ell}{\mathbf{T}_\ell \cdot \mathbf{T}_\ell} = \frac{1}{i\omega\epsilon_0\epsilon^{(w)}} \frac{(\partial_N w)}{|\mathbf{T}_\ell|^2} = \frac{1}{i\omega\epsilon_0\epsilon^{(w)}} \frac{(\partial_N w)}{|\mathbf{N}|^2}.$$

Thus we have

$$|\mathbf{N}| \frac{\sigma^{(g)}}{i\omega\epsilon_0\epsilon^{(w)}} \frac{(\partial_N w)}{|\mathbf{N}|^2} \mathbf{T}_\ell = |\mathbf{N}| \sigma^{(g)} \left(\frac{\mathbf{E}^{(w)} \cdot \mathbf{T}_\ell}{\mathbf{T}_\ell \cdot \mathbf{T}_\ell} \right) \mathbf{T}_\ell = |\mathbf{N}| \mathbf{j}_s = \mathbf{N} \times \mathbf{H} = (-v) \mathbf{T}_\ell,$$

and we find

$$|\mathbf{N}| (i\omega\epsilon_0)u - \left[-\frac{\sigma^{(g)}}{\epsilon^{(w)}} \partial_N + |\mathbf{N}| (i\omega\epsilon_0) \right] w = -|\mathbf{N}| (i\omega\epsilon_0)u^i \quad \text{at } z = g(x).$$

Dividing by $(i\omega\epsilon_0)$ and again using the facts that $\omega = c_0 k_0$ and $\sigma^{(g)} = \epsilon_0 c_0 \hat{\sigma}^{(g)}$, this simplifies to

$$|\mathbf{N}| u - [|\mathbf{N}| - \eta \partial_N] w = -|\mathbf{N}| u^i \quad \text{at } z = g(x)$$

where

$$\eta = \eta(\omega) := \frac{\sigma^{(g)}}{i\omega\epsilon_0\epsilon^{(w)}} = \frac{\hat{\sigma}^{(g)}}{ik_0\epsilon^{(w)}}.$$

We gather these results and state that we seek *quasiperiodic, outgoing* solutions of

$$(2.7a) \quad \Delta u + \epsilon^{(u)} k_0^2 u = 0, \quad z > g(x),$$

$$(2.7b) \quad \Delta w + \epsilon^{(w)} k_0^2 w = 0, \quad z < g(x),$$

$$(2.7c) \quad |\mathbf{N}| u - [|\mathbf{N}| - \eta \partial_N] w = |\mathbf{N}| \zeta \quad \text{at } z = g(x),$$

$$(2.7d) \quad \partial_N u - \tau^2 \partial_N w = \psi \quad \text{at } z = g(x),$$

where ζ and ψ are defined in (2.6e).

3. Surface formulation via Dirichlet–Neumann operators. We now seek to equivalently reformulate the governing equations of TE, (2.6), and TM, (2.7), polarization in terms of boundary unknowns and operators. For this we introduce the Dirichlet traces

$$U(x) := u(x, g(x)), \quad W(x) := w(x, g(x)),$$

and their outward pointing Neumann counterparts

$$\tilde{U}(x) := -(\partial_N u)(x, g(x)), \quad \tilde{W}(x) := (\partial_N w)(x, g(x)).$$

Of great importance to our formulation will be the DNOs which map the former to the latter. To be more precise, given the unique α -quasiperiodic,

$$u(x + d, z) = e^{i\alpha d} u(x, z),$$

the upward-propagating [60, 3] solution to the elliptic boundary value problem

$$(3.1a) \quad \Delta u + \epsilon^{(u)} k_0^2 u = 0, \quad z > g(x),$$

$$(3.1b) \quad u(x, g(x)) = U(x), \quad z = g(x),$$

the DNO is defined as the map

$$(3.2) \quad G(g) : U(x) \rightarrow \tilde{U}(x).$$

In a similar manner, given the unique α -quasiperiodic, downward-propagating solution to the elliptic boundary value problem

$$(3.3a) \quad \Delta w + \epsilon^{(w)} k_0^2 w = 0, \quad z < g(x),$$

$$(3.3b) \quad w(x, g(x)) = W(x), \quad z = g(x),$$

the DNO is defined as

$$(3.4) \quad J(g) : W(x) \rightarrow \tilde{W}(x).$$

In the case of a flat interface, $g \equiv 0$, it is easy to find G and J from the Rayleigh expansions [60, 71]

$$(3.5) \quad u(x, z) = \sum_{p=-\infty}^{\infty} \hat{u}_p e^{i\alpha_p x + i\gamma_p^{(u)} z}, \quad w(x, z) = \sum_{p=-\infty}^{\infty} \hat{w}_p e^{i\alpha_p x - i\gamma_p^{(w)} z},$$

where, for $m \in \{u, w\}$,

$$\alpha_p := \alpha + \left(\frac{2\pi}{d}\right) p, \quad \gamma_p^{(m)} := \begin{cases} \sqrt{\epsilon^{(m)} k_0^2 - \alpha_p^2}, & p \in \mathcal{U}^{(m)}, \\ i\sqrt{\alpha_p^2 - \epsilon^{(m)} k_0^2}, & p \notin \mathcal{U}^{(m)}, \end{cases}$$

and

$$\mathcal{U}^{(m)} := \left\{ p \in \mathbf{Z} \mid \alpha_p^2 < \epsilon^{(m)} k_0^2 \right\}$$

are the propagating modes. From these expansions we see that

$$(3.6) \quad G(0)U = \sum_{p=-\infty}^{\infty} (-i\gamma_p^{(u)}) \hat{U}_p e^{i\alpha_p x}, \quad J(0)W = \sum_{p=-\infty}^{\infty} (-i\gamma_p^{(w)}) \hat{W}_p e^{i\alpha_p x}.$$

3.1. TE polarization. In terms of these DNOs, the TE equations, (2.6), can be shown to be *equivalent* to the boundary equations

$$\begin{aligned} U - W &= \zeta, \\ -\tilde{U} - \tilde{W} + |\mathbf{N}| \rho W &= \psi. \end{aligned}$$

Using the DNOs defined above, (3.2) and (3.4), we can rewrite the equations above as

$$\begin{aligned} U - W &= \zeta, \\ -G[U] - J[W] + |\mathbf{N}| \rho W &= \psi. \end{aligned}$$

We rearrange this to read

$$(3.7) \quad \begin{pmatrix} I & -I \\ G & J - |\mathbf{N}| \rho I \end{pmatrix} \begin{pmatrix} U \\ W \end{pmatrix} = \begin{pmatrix} \zeta \\ -\psi \end{pmatrix},$$

which can be compared with (C.2) in Appendix C, obtained by a vanishing layer thickness argument.

3.2. TM polarization. On the other hand, the TM equations, (2.7), are *equivalent* to the boundary equations

$$\begin{aligned} |\mathbf{N}| U - |\mathbf{N}| W + \eta \tilde{W} &= |\mathbf{N}| \zeta, \\ -\tilde{U} - \tau^2 \tilde{W} &= \psi, \end{aligned}$$

which we can rewrite as

$$\begin{aligned} |\mathbf{N}| U - |\mathbf{N}| W + \eta J[W] &= |\mathbf{N}| \zeta, \\ -G[U] - \tau^2 J[W] &= \psi. \end{aligned}$$

We rearrange this to read

$$(3.8) \quad \begin{pmatrix} |\mathbf{N}| & -|\mathbf{N}| + \eta J \\ G & \tau^2 J \end{pmatrix} \begin{pmatrix} U \\ W \end{pmatrix} = \begin{pmatrix} |\mathbf{N}| \zeta \\ -\psi \end{pmatrix},$$

which can again be compared with the vanishing layer thickness result (C.3) in Appendix C.

4. Surface Plasmon Resonances. We are now in a position to search for the surface waves which deliver field enhancements at the interface of the three materials. For noble metals these are induced by a classical SPR and we seek an analogue of this condition in the present context. Following [49] the condition for an SPR is the singularity of the linearized operator (flat interface) in the governing equations. More specifically, for a TE SPR we require that

$$M^{\text{TE}} := \begin{pmatrix} I & -I \\ G(0) & J(0) - \rho I \end{pmatrix}$$

be singular, while for a TM SPR we demand that

$$M^{\text{TM}} := \begin{pmatrix} I & -I + \eta J(0) \\ G(0) & \tau^2 J(0) \end{pmatrix}$$

be noninvertible. Using the periodicity of the solutions

$$U(x) = \sum_{p=-\infty}^{\infty} \hat{U}_p e^{i\alpha_p x}, \quad W(x) = \sum_{p=-\infty}^{\infty} \hat{W}_p e^{i\alpha_p x}$$

and the forms (3.6), we find that we must consider singularities of the operators

$$\widehat{M}^{\text{TE}}_p := \begin{pmatrix} 1 & -1 \\ (-i\gamma_p^{(u)}) & (-i\gamma_p^{(w)}) - \rho \end{pmatrix}$$

and

$$\widehat{M}^{\text{TM}}_p := \begin{pmatrix} 1 & -1 + \eta(-i\gamma_p^{(w)}) \\ (-i\gamma_p^{(u)}) & \tau^2(-i\gamma_p^{(w)}) \end{pmatrix}.$$

We measure this singularity with the determinant functions

$$\begin{aligned} \left(\widetilde{\Delta}^{\text{TE}}\right)_p &= (-i\gamma_p^{(u)}) + (-i\gamma_p^{(w)}) - \rho, \\ \left(\widetilde{\Delta}^{\text{TM}}\right)_p &= (-i\gamma_p^{(u)}) + \tau^2(-i\gamma_p^{(w)}) - \eta(-i\gamma_p^{(u)})(-i\gamma_p^{(w)}). \end{aligned}$$

A little manipulation delivers two alternative determinant functions with the same zeros,

$$(4.1a) \quad \Delta_p^{\text{TE}} = \gamma_p^{(u)} + \gamma_p^{(w)} + \omega\mu_0\sigma^{(g)} = \gamma_p^{(u)} + \gamma_p^{(w)} + k_0\hat{\sigma}^{(g)},$$

$$(4.1b) \quad \Delta_p^{\text{TM}} = \frac{\epsilon^{(u)}}{\gamma_p^{(u)}} + \frac{\epsilon^{(w)}}{\gamma_p^{(w)}} + \frac{\sigma^{(g)}}{\omega\epsilon_0} = \frac{\epsilon^{(u)}}{\gamma_p^{(u)}} + \frac{\epsilon^{(w)}}{\gamma_p^{(w)}} + \frac{\hat{\sigma}^{(g)}}{k_0}.$$

We now consider the case of graphene and the model of the induced surface current specified in Appendix B. We plot the functions Δ_p^{TE} and Δ_p^{TM} for $p = 0, 1, 2, 3, 4$ (with $d = 0.600$ microns) and values of the chemical potential $\mu = 0.3$ (Figures 2(a) and 2(b)), $\mu = 0.4$ (Figures 3(a) and 3(b)), $\mu = 0.5$ (Figures 4(a) and 4(b)), showing not only the possibility of resonance in TM polarization for λ sufficiently large (the terahertz and infrared regime), but also the lack of evidence for resonance in TE polarization (as with classical SPRs [62]). We note that there appears to be no possibility of a zero for $p = 0$ in either polarization meaning that plasmons cannot be excited by a flat dielectric-graphene-dielectric (DGD) structure. However, for $p \neq 0$ there are near-zeros indicating the possibility of launching a surface plasmon from a *corrugated* DGD structure. We will soon focus on the near-zeros associated with $p = 1$, as these responses will be the strongest, which occur at

$$(4.2) \quad \begin{aligned} \lambda_{\text{SPR},0.3} &\approx 18.81 \text{ microns}, & \lambda_{\text{SPR},0.4} &\approx 16.29 \text{ microns}, \\ \lambda_{\text{SPR},0.5} &\approx 14.58 \text{ microns}. \end{aligned}$$

5. Numerical simulation of the DNOs. In order to perform a numerical simulation of (3.7) and (3.8), one specification remains to be made: How to approximate the DNOs G and J . There is a large literature on the efficient, stable, and accurate numerical computation of DNOs. We follow the HOPS philosophy pursued in a long

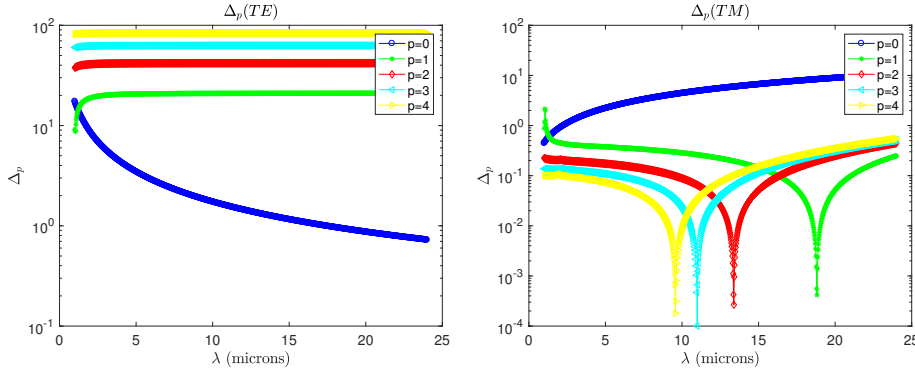


FIG. 2. Plot of Δ_p in (a) TE and (b) TM configurations for $\mu = 0.3$.

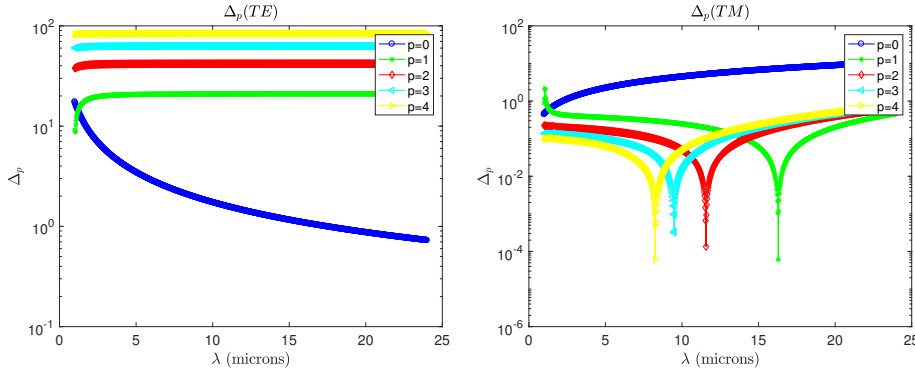


FIG. 3. Plot of Δ_p in (a) TE and (b) TM configurations for $\mu = 0.4$.

line of research [51, 52, 53] (regarding Laplace’s equation), [54, 55, 56, 43, 37, 29, 45] (regarding the Helmholtz equation), and [50, 46] (regarding the Maxwell equations); see also [57, 49]. In brief, the approach begins with the assumption that the shape of the interface deformation $g(x)$ satisfies

$$g(x) = \varepsilon f(x), \quad \varepsilon \ll 1,$$

with f sufficiently smooth (for a rigorous proof in the case of C^2 profiles, see [51, 55], while Lipschitz interfaces are considered in [30]). We point out that the smallness assumption on ε can be removed by analytic continuation, rigorously justified in [53, 31] and numerically implemented via Padé summation [11, 52, 55]. With this assumption the DNOs can be shown to depend *analytically* upon the deformation size ε so that

$$G = G(\varepsilon f) = \sum_{n=0}^{\infty} G_n(f) \varepsilon^n, \quad J = J(\varepsilon f) = \sum_{n=0}^{\infty} J_n(f) \varepsilon^n.$$

The question now becomes: Can useful forms for the $\{G_n, J_n\}$ can be derived? We briefly describe two approaches here: The FE due to Bruno and Reitich [10, 11, 12], and the TFE devised by Nicholls and Reitich [51, 55].

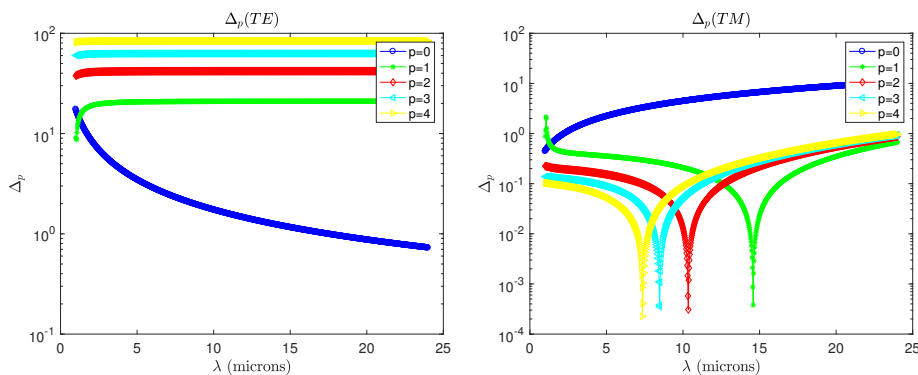


FIG. 4. Plot of Δ_p in (a) TE and (b) TM configurations for $\mu = 0.5$.

5.1. Field expansions. The FE in the current context begins with the supposition (verified a posteriori) that the scattered fields also depend analytically upon ε . Focusing upon the field in the upper layer, $\{z > g(x)\}$, this implies that

$$u = u(x, z; \varepsilon) = \sum_{n=0}^{\infty} u_n(x, z) \varepsilon^n.$$

Upon insertion of this into (3.1) one finds that the u_n must be α -quasiperiodic, upward-propagating solutions of the elliptic boundary value problem

$$(5.1a) \quad \Delta u_n + \varepsilon^{(u)} k_0^2 u_n = 0, \quad z > 0,$$

$$(5.1b) \quad u_n(x, 0) = \delta_{n,0} U(x) - \sum_{\ell=0}^{n-1} \frac{f(x)^{n-\ell}}{(n-\ell)!} \partial_z^{n-\ell} v_\ell(x, 0), \quad z = 0,$$

where $\delta_{n,\ell}$ is the Kronecker delta function. The classical Rayleigh expansions [60, 71] (cf. (3.5)) provide solutions

$$u_n(x, z) = \sum_{p=-\infty}^{\infty} \hat{u}_{n,p} e^{i\alpha_p x + i\gamma_p^{(u)} z},$$

and the $\hat{u}_{n,p}$ are determined recursively from the boundary conditions, (5.1b), beginning, at order zero, with the Fresnel coefficients

$$\hat{u}_{0,p} = \hat{U}_p.$$

From this the DNO, (3.2), can be computed from

$$G = -\partial_N u(x, \varepsilon f) = \sum_{n=0}^{\infty} \sum_{p=-\infty}^{\infty} (-i\gamma_p^{(u)} + \varepsilon(\partial_x f) i\alpha_p) \hat{u}_{n,p} e^{i\alpha_p x} e^{i\gamma_p^{(u)} \varepsilon f} \varepsilon^n,$$

expanding the exponential $\exp(i\gamma_p^{(u)} \varepsilon f)$ in a power series in ε , and equating like powers of ε . Similar considerations hold for the DNO J save that the alternate Rayleigh

expansion (cf. (3.5))

$$w_n(x, z) = \sum_{p=-\infty}^{\infty} \hat{w}_{n,p} e^{i\alpha_p x - i\gamma_p^{(w)} z}$$

must be used.

5.2. Transformed field expansions. The TFE method proceeds in exactly the same manner as the FE approach save that a “domain–flattening” change of variables is affected before the expansion in ε is made. This change of variables is well known in the literature and goes by the name σ -coordinates in the atmospheric sciences [61], and the C-Method in the theory of gratings [15]. The change of variables essentially amounts to

$$x' = x, \quad z' = z - g(x),$$

which not only maps the deformed interface shape $\{z = g(x)\}$ to the trivial shape $\{z' = 0\}$, but also results in a greatly stabilized sequence of recursions. For complete details together with numerical validation, please see, e.g., [55]. The downside of this approach is the slightly elevated computational cost due to the fact that this change of variables introduces inhomogeneities into the governing equations, e.g.,

$$\begin{aligned} \Delta' u' + \epsilon^{(u)} k_0^2 u' &= F(x', z'), & z' > 0, \\ u'(x', 0) &= U(x'), & z' = 0. \end{aligned}$$

This means that the Rayleigh expansions cannot be used directly and a *volumetric* discretization is required [52, 55]. However, the greatly enhanced stability and applicability (large and rough deformations can be readily simulated) oftentimes make this extra cost worthwhile.

6. A High-Order Perturbation of Surfaces method. In light of the developments in the previous section regarding the computation of DNOs we can now describe a rapid, highly accurate, and stable algorithm to compute solutions to the surface TE, (3.7), and TM, (3.8), equations. In the interest of brevity we describe our approach for the TE polarization alone as the TM version is quite similar.

Again, making the HOPS assumption $g(x) = \varepsilon f(x)$, we suppose not only that the DNO depend analytically upon ε but also that the surface fields do as well, so that

$$U = U(x; \varepsilon) = \sum_{n=0}^{\infty} U_n(x) \varepsilon^n, \quad W = W(x; \varepsilon) = \sum_{n=0}^{\infty} W_n(x) \varepsilon^n.$$

Upon insertion of these into (3.7), equating at like orders delivers, at order zero,

$$(6.1) \quad \begin{pmatrix} I & -I \\ G_0 & J_0 - \rho I \end{pmatrix} \begin{pmatrix} U_0 \\ W_0 \end{pmatrix} = \begin{pmatrix} \zeta_0 \\ -\psi_0 \end{pmatrix}.$$

At higher orders we find

$$(6.2) \quad \begin{pmatrix} I & -I \\ G_0 & J_0 - \rho I \end{pmatrix} \begin{pmatrix} U_n \\ W_n \end{pmatrix} = \begin{pmatrix} \zeta_n \\ R_n \end{pmatrix},$$

where

$$R_n = -\psi_n - \sum_{\ell=0}^{n-1} (G_{n-\ell}[U_\ell] + J_{n-\ell}[W_\ell] - \rho |N|_{n-\ell} W_\ell)$$

and

$$|N| = |N|(x; \varepsilon) = \sum_{n=0}^{\infty} |N|_n(x) \varepsilon^n.$$

Appealing to our simple formulas for $G_0 = G(0)$ and $J_0 = J(0)$, (3.6), and using the Fourier expansions

$$U_n(x) = \sum_{p=-\infty}^{\infty} \hat{U}_{n,p} e^{i\alpha_p x}, \quad W_n(x) = \sum_{p=-\infty}^{\infty} \hat{W}_{n,p} e^{i\alpha_p x},$$

we realize that both (6.1) and (6.2) can be solved very rapidly by the Fast Fourier Transform (FFT) algorithm [52, 55]. Once these $\{\hat{U}_{n,p}, \hat{W}_{n,p}\}$ are recovered we can form, for instance, approximations of the surface fields

$$U^N(x; \varepsilon) := \sum_{n=0}^N \sum_{p=-\infty}^{\infty} \hat{U}_{n,p} e^{i\alpha_p x} \varepsilon^n, \quad W^N(x; \varepsilon) := \sum_{n=0}^N \sum_{p=-\infty}^{\infty} \hat{W}_{n,p} e^{i\alpha_p x} \varepsilon^n.$$

We note that one may choose among several methods to sum the truncated Taylor series (in n) which appear above. In addition to direct (Taylor) summation, the classical numerical analytic continuation method of Padé approximation [5] has been very successful when applied to HOPS algorithms [11, 53, 55, 57]. The Padé approximant has remarkable properties; among these are that, for a wide class of functions, not only is the convergence *faster* at points of analyticity, but also it may converge for points *outside* the disk of convergence. We refer the reader to section 2.2 of Baker and Graves-Morris [5] and section 8.3 of Bender and Orszag [8] for a complete discussion of the capabilities and limitations of Padé approximants.

7. Numerical results. Now that we have a mathematical framework in place, together with a computational algorithm to simulate solutions, we would like to approximate a configuration of interest to engineers. With the recent explosion of attention to graphene and its use in nano-optical devices, there are many from which to choose. Based upon the work of the group of T. Low at the University of Minnesota, we select a geometry inspired by one of the devices they have studied.

It is well known not only that the optical response of graphene is typically *outside* the visible region, but also that the effect for a uniform flat layer can be quite weak. However, the Low group has shown that with periodic *patterning* this effect can be made much more dramatic [34, 70, 14, 20, 64]; furthermore, with sufficient chemical or electrical gating, free carriers can be induced with ease, thereby changing the value of the chemical potential, μ (see Appendix B), quite drastically.

In [14] the Low group investigated the possibility of plasmonic excitation with *strips* of graphene deposited on a solid dielectric substrate, overlaid with an electrolyte gating superstrate. With this basic configuration (there are other features which must be added; see [14] for full details) their group was able to construct a device which could manipulate the phase shift of reflected light based upon the periodicity of the striping, and the chemical potential, μ , generated by the electrolyte.

Their geometry features only flat interfaces in the layers of the structure so a method such as ours is unnecessary (the authors resorted to a full Finite Element simulation). However, it is easy to imagine how our computational capability can easily be brought to bear upon slightly different configurations to illuminate other

interesting behavior. More specifically, we note that the *patterning* and *periodicity* of the strip deposition is what generates the strong response noted by Low. We mimic this mechanism by retaining a solid layer of graphene, but perturbing the *geometry* in the same manner that classical SPRs are generated by a corrugated interface [62, 36, 19] in TM polarization.

With this in mind we consider a doubly layered structure (e.g., depicted in Figure 1) where dielectrics occupy the layers S^u and S^w (cf. (2.2)) separated by a *non-trivial* interface shaped by $z = g(x) = \varepsilon f(x)$, (2.1). At this interface we place a layer of graphene and study the reflectivity map induced by plane-wave illumination in TM polarization as the size, ε , of g is varied.

7.1. Validation by the method of manufactured solutions. Before proceeding to our numerical simulations, we validate our code using the Method of Manufactured Solutions (MMS) [13, 63, 65]. To summarize the MMS, when solving a system of partial differential equations subject to boundary conditions for an unknown, v , say

$$(7.1a) \quad \mathcal{P}v = 0 \quad \text{in } \Omega,$$

$$(7.1b) \quad \mathcal{B}v = 0 \quad \text{at } \partial\Omega,$$

it is typically just as easy to implement an algorithm to solve the “inhomogeneous” version of the above,

$$(7.2a) \quad \mathcal{P}v = \mathcal{F} \quad \text{in } \Omega,$$

$$(7.2b) \quad \mathcal{B}v = \mathcal{J} \quad \text{at } \partial\Omega.$$

In order to test a code, one begins with the “manufactured solution,” \tilde{v} , and sets

$$\mathcal{F}_{\tilde{v}} := \mathcal{P}\tilde{v}, \quad \mathcal{J}_{\tilde{v}} := \mathcal{B}\tilde{v}.$$

Now, given this pair $\{\mathcal{F}_{\tilde{v}}, \mathcal{J}_{\tilde{v}}\}$ we have an *exact* solution to (7.2) against which we can compare our numerically simulated solution. While this provides no guarantee of a correct implementation, with a careful choice of \tilde{v} , e.g., one which displays the same qualitative behavior as solutions of (7.1), the approach can give great confidence in the accuracy of a scheme.

For the implementation in question we consider the α -quasiperiodic, outgoing solutions of the Helmholtz equation, (3.1),

$$u^r(x, z) = A_u^r e^{i\alpha_r x + i\gamma_r^{(u)} z}, \quad r \in \mathbf{Z}, \quad A_u^r \in \mathbf{C},$$

and the counterpart for (3.3),

$$w^r(x, z) = A_w^r e^{i\alpha_r x - i\gamma_r^{(w)} z}, \quad r \in \mathbf{Z}, \quad A_w^r \in \mathbf{C}.$$

For the interface shape we select the periodic and analytic function

$$f(x) = e^{\cos(x)},$$

and from these we can compute, e.g., the exact surface current

$$\nu^{\text{ex}}(x) := [\partial_N u^r - \partial_N w^r]_{z=\varepsilon f(x)}.$$

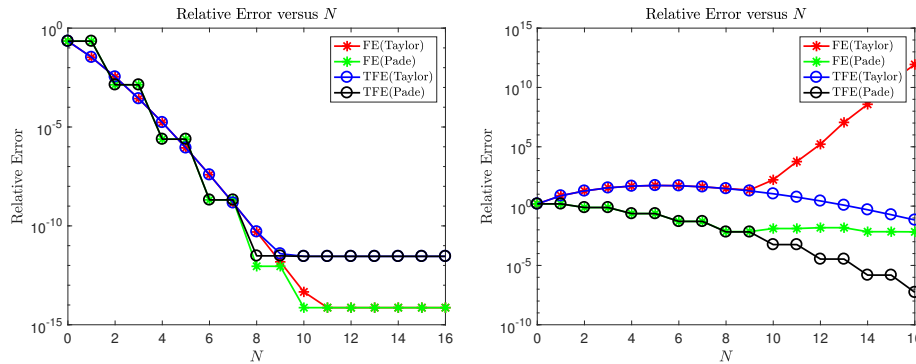


FIG. 5. Relative error (7.4) versus perturbation order for configuration (7.3) with (a) $\varepsilon = d/100$ and (b) $\varepsilon = d/5$; FE and TFE schemes with Taylor and Padé summation.

We make the physical parameter choices

$$(7.3a) \quad r = 2, \quad A_u^r = -3, \quad A_w^r = 4, \quad \rho = -2 + i, \quad \eta = 3 - 2i, \quad d = 2\pi$$

and numerical parameter choices

$$(7.3b) \quad N_x = 32, \quad N_z = 16, \quad a = 0.5, \quad b = 0.5, \quad N = 16$$

and compute approximations to ν^{ex} by the FE and TFE algorithms delivering ν^{FE} and ν^{TFE} , respectively. (The parameters a and b specify locations of artificial boundaries in the TFE formulation, while N_z gives the spatial discretization in the vertical direction; please see [55, 44] for full details.) We measure the relative error

$$(7.4) \quad \text{Error}_{\text{rel}}^{\text{FE}} = \frac{|\nu^{\text{ex}} - \nu_{N_x, N}^{\text{FE}}|_{L^\infty}}{|\nu^{\text{ex}}|_{L^\infty}}, \quad \text{Error}_{\text{rel}}^{\text{TFE}} = \frac{|\nu^{\text{ex}} - \nu_{N_x, N_z, N}^{\text{TFE}}|_{L^\infty}}{|\nu^{\text{ex}}|_{L^\infty}}$$

and display our results in Figure 5(a) for $\varepsilon = d/100$. Here we see the precipitous (spectral) convergence of our method to the true solution down to machine precision (up to the conditioning of our algorithms [53]) by ten perturbation orders. We revisit this calculation in the vastly more challenging case $\varepsilon = d/5$ with the modifications that $N_x = 256$, $N_z = 64$, and $a = b = 2$. The results are displayed in Figure 5(b) and show the extremely beneficial effects of not only the stabilized TFE approach [52], but also Padé summation [53].

7.2. Validation by comparison to results in the literature. As a second validation of our method we revisit a simulation appearing in the literature with our own algorithm. For this we choose the survey paper of Bludov et al. [9], in particular the calculations presented in section 9 (“Scattering of ER from corrugated graphene”) and section 9.4 (“A nontrivial example I: sine profile”) where they study scattering by a one-dimensional, sinusoidally perturbed graphene sheet in TM polarization. More specifically, they study an interface profile (where the graphene exists) shaped by

$$g(x) = \varepsilon \sin(2\pi x/d),$$

where we have used the notation of the present contribution. Beyond this, they make the physical parameter choices

$$d = 10 \text{ microns}, \quad \epsilon^{(u)} = 1, \quad \epsilon^{(w)} = 11, \quad \alpha = 0,$$

and use a Drude model for the graphene

$$\sigma_D = \sigma_0 \left(\frac{4E_F}{\pi} \right) \frac{1}{\hbar\gamma - i\hbar\omega}, \quad \sigma_0 = \frac{\pi e^2}{2h},$$

where $e < 0$ is the electron charge, γ is the relaxation rate, and $E_F > 0$ is the (local) Fermi level position. In [9] the authors chose values $E_F = 0.45$ eV and $\hbar\gamma =: \Gamma = 2.6$ meV.

With these values the authors plotted curves of (specular) reflectance, transmission, and absorbance,

$$R_0 = |\hat{u}_0|^2, \quad T_0 = (\gamma^{(w)}/\gamma^{(u)}) |\hat{w}_0|^2, \quad A_0 = 1 - R_0 - T_0,$$

respectively, versus energy of the incident radiation, $E = hc_0/\lambda$, for four choices of the interface height

$$\varepsilon = d/100, d/25, d/15, d/10.$$

We reproduced these with our new HOPS methodology and display the results in Figures 6(a), 6(b), and 6(c). We point out the remarkable *qualitative* agreement, including the SPR excited around 11 meV as predicted in [9].

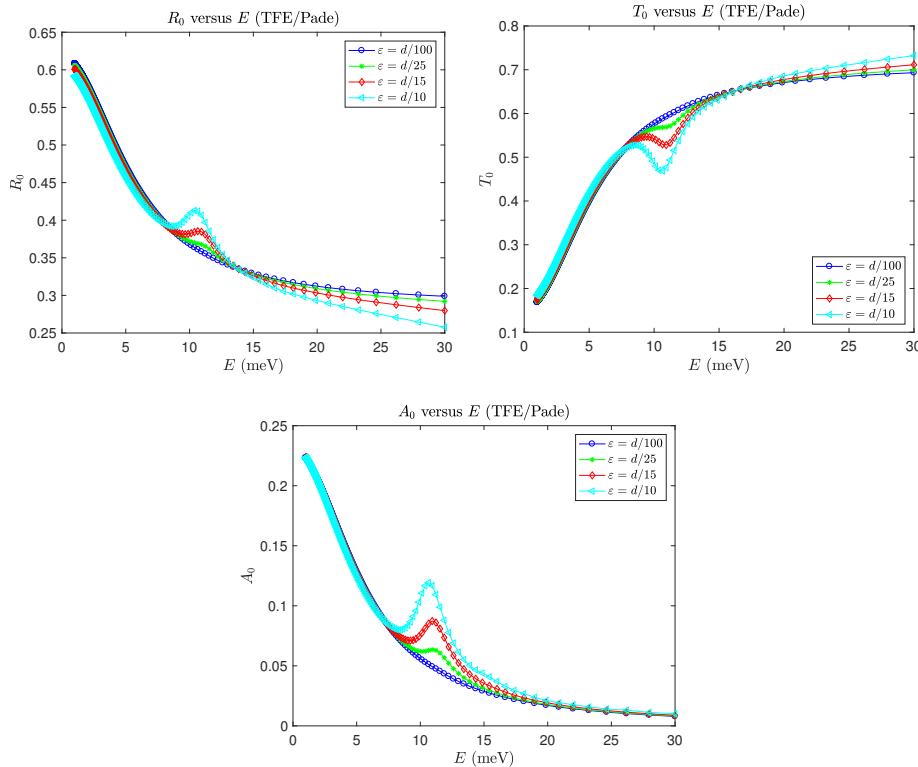


FIG. 6. (a) Specular reflectance, R_0 , (b) specular transmission, T_0 , and (c) specular absorbance, A_0 , versus energy for four choices of the interface height, $\varepsilon = d/100, d/25, d/15, d/10$ with $d = 10$ microns. HOPS method with $N_x = 128$, $N_z = 32$, and $N = 8$.

7.3. Wavy nanosheets. Having verified the accuracy and validity of our code in the previous sections, we use it to simulate the configuration outlined at the beginning of section 7. We recall that this is a contiguous, corrugated layer of graphene shaped by $z = g(x)$, sandwiched between two semi-infinite dielectric layers. To specify a particular configuration we select $f(x) = \cos(2\pi x/d)$ ($d = 0.600$ microns), vacuum ($n^{(u)} = 1$) above the layer of graphene, and alumina ($n^{(w)} = 1.76$) below.

To simulate the electric gating, which can be induced in graphene layers, we vary the chemical potential μ . Many values appear in the literature for this constant, but those between 0.1 eV and 0.5 eV are commonplace [4, 34, 70, 14, 20, 64, 2]. For the purpose of our simulations, we study three values within this range ($\mu = 0.3, 0.4, 0.5$) and show how, in TM configuration, the strongest plasmonic response (associated to wavenumber $p = 1$) can be moved quite significantly with variation of the chemical potential; cf. (4.2).

To measure this we study the Reflectivity Map which we define in terms of the Rayleigh expansions for the reflected and transmitted fields (cf. (3.5)),

$$u(x, z) = \sum_{p=-\infty}^{\infty} \hat{u}_p e^{i\alpha_p x + i\gamma_p^{(u)} z}, \quad w(x, z) = \sum_{p=-\infty}^{\infty} \hat{w}_p e^{i\alpha_p x - i\gamma_p^{(w)} z},$$

respectively. In terms of these the efficiencies are defined as

$$e_p^{(u)} := \left(\frac{\gamma_p^{(u)}}{\gamma^{(u)}} \right) |\hat{u}_p|^2, \quad e_p^{(w)} := \left(\frac{\gamma_p^{(w)}}{\gamma^{(w)}} \right) |\hat{w}_p|^2,$$

and the Reflectivity Map is defined by

$$(7.5) \quad R(\lambda, \varepsilon) := \sum_{p \in \mathcal{U}^{(u)}} e_p^{(u)}.$$

We begin with the value $\mu = 0.3$ eV and display results of our simulation of the normalized Reflectivity Map, $R(\lambda, \varepsilon)/R(\lambda, 0)$, in Figure 7(a), together with the final slice of this at $\varepsilon = d/10$ in Figure 7(b). Due to the very strong and extremely confined plasmonic response, in order to make Figures 7(a), 8(a), and 9(a) more readable we actually plot $\min\{R(\lambda, \varepsilon)/R(\lambda, 0), 2\}$. In this simulation we have chosen

$$N_x = 96, \quad N_z = 48, \quad a = 1, \quad b = 1, \quad N = 20,$$

which differs, in the supremum norm, from the Reflectivity Map computed with $N_x = 64$, $N_z = 32$, and $N = 16$ by 10^{-6} . We note the *dramatic* shift that one can realize by introducing a corrugation into the graphene layer. Here we see that the SPR has moved from roughly 18.81 microns to 20.1 microns; cf. (4.2).

We revisit this simulation (with the same numerical parameters) in the case $\mu = 0.4$ eV, and in Figure 8(a) show $R(\lambda, \varepsilon)/R(\lambda, 0)$. Again, we display the final slice of this at $\varepsilon = d/10$ in Figure 8(b). As before, there is a *sizable* shift in the location of the SPR with a corrugation in the graphene layer. Now the SPR has moved from roughly 16.29 microns to 17.4 microns; cf. (4.2).

Finally, we consider the case $\mu = 0.5$ eV (again, with the same numerical parameters). In Figure 9(a) we display $R(\lambda, \varepsilon)/R(\lambda, 0)$ and in Figure 9(b) we show the final slice of this at $\varepsilon = d/10$. As before, there is a *huge* shift in the location of the SPR with a corrugation in the graphene layer. Now the SPR has moved from roughly 14.58 microns to 15.5 microns; cf. (4.2).

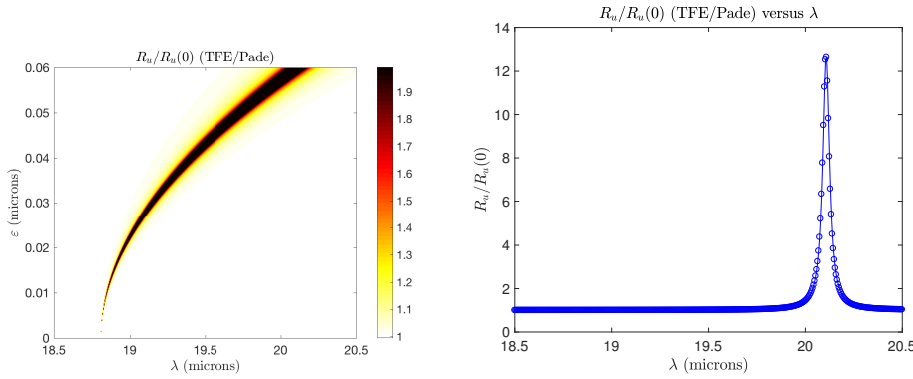


FIG. 7. (a) Contour plot of the Reflectivity Map and (b) its final slice for $\mu = 0.3$.

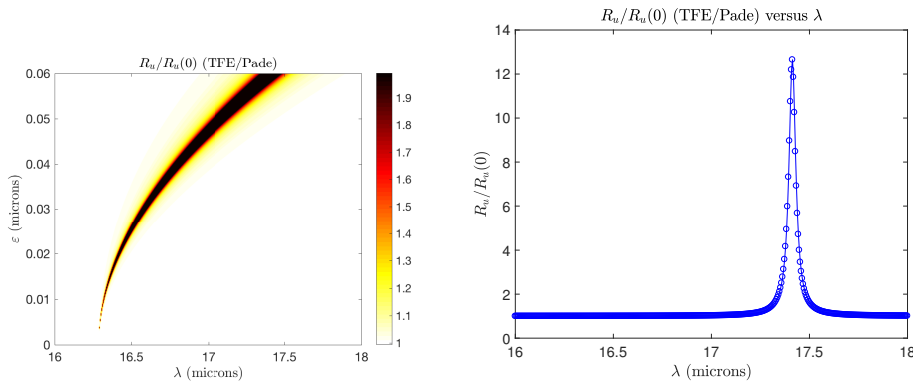


FIG. 8. (a) Contour plot of the Reflectivity Map and (b) its final slice for $\mu = 0.4$.

Before closing, we highlight the fact that with a *fixed* geometry (fixed value of ϵ), the location of the SPR can be moved conveniently and quickly by changing μ . For instance, by fixing $\epsilon = d/10$ the SPR can be moved among

$$\begin{aligned} \lambda_{\text{SPR},0.3}(d/10) &\approx 20.1 \text{ microns}, & \lambda_{\text{SPR},0.4}(d/10) &\approx 17.4 \text{ microns}, \\ \lambda_{\text{SPR},0.5}(d/10) &\approx 15.5 \text{ microns}, \end{aligned}$$

as μ is varied.

Appendix A. Derivation of Helmholtz equations. In this appendix we provide details of the derivation of the governing Helmholtz equations which appear in TM polarization (the TE case is analogous). We remember that

$$\mathbf{H}(x, z) = \begin{pmatrix} 0 & v(x, z) & 0 \end{pmatrix}^T = v(x, z)\mathbf{T}_t,$$

from which we can compute

$$\text{curl}[\mathbf{H}(x, z)] = \begin{pmatrix} -\partial_z v(x, z) & 0 & \partial_x v(x, z) \end{pmatrix}^T.$$

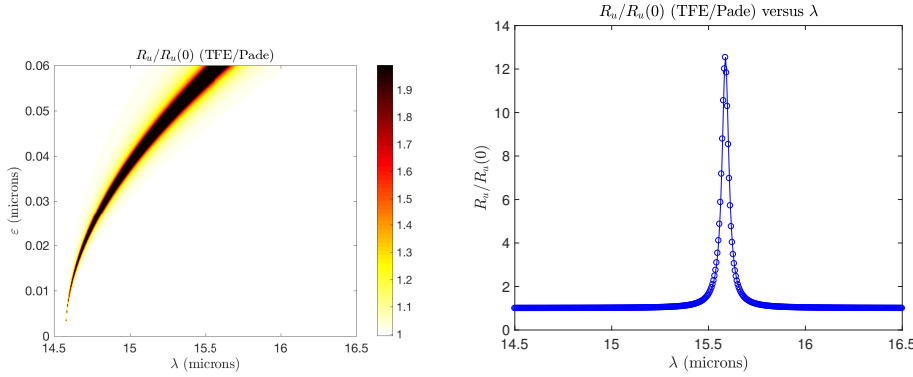


FIG. 9. (a) Contour plot of the Reflectivity Map and (b) its final slice for $\mu = 0.5$.

From (2.3b) we find that

$$\begin{aligned} \mathbf{E}(x, z) &= -\frac{1}{i\omega\epsilon_0\epsilon} \operatorname{curl}[\mathbf{H}(x, z)] = -\frac{1}{i\omega\epsilon_0\epsilon} \begin{pmatrix} -\partial_z v(x, z) & 0 & \partial_x v(x, z) \end{pmatrix}^T \\ &=: \begin{pmatrix} E^x(x, z) & 0 & E^z(x, z) \end{pmatrix}^T, \end{aligned}$$

and we can compute

$$\operatorname{curl}[\mathbf{E}(x, z)] = \begin{pmatrix} 0 & (\partial_z E^x(x, z) - \partial_x E^z(x, z)) & 0 \end{pmatrix}^T = \operatorname{div} \left[\frac{1}{i\omega\epsilon_0\epsilon} \nabla v \right] \mathbf{T}_t.$$

Now (2.3a) demands that

$$i\omega\mu_0 v(x, z) \mathbf{T}_t = i\omega\mu_0 \mathbf{H}(x, z) = \operatorname{curl}[\mathbf{E}(x, z)] = \operatorname{div} \left[\frac{1}{i\omega\epsilon_0\epsilon} \nabla v(x, z) \right] \mathbf{T}_t,$$

which implies, since ϵ jumps from S^u to S^w , that

$$\operatorname{div} \left[\frac{1}{\epsilon} \nabla v \right] + k_0^2 v = 0,$$

where $k_0^2 = \omega^2 \epsilon_0 \mu_0$.

Appendix B. The surface conductivity of graphene. We now describe one popular approach to modeling the surface conductivity induced at a graphene layer. We follow the lead of [4, 2] who utilize the approximation of Stauber, Peres, and Neto [67]. To begin we define the dimensionless function $\hat{\sigma}^{(g)} = \hat{\sigma}_r^{(g)} + i\hat{\sigma}_i^{(g)}$ where

$$\begin{aligned} \hat{\sigma}_r^{(g)} &:= \pi\alpha\eta_\ell \left\{ \frac{\tanh((\Omega + 2)/\kappa) + \tanh((\Omega - 2)/\kappa)}{2} \right\}, \\ \hat{\sigma}_i^{(g)} &:= \frac{4\alpha}{\Omega} \left(1 - \frac{2\mu^2}{9t^2} \right) + \alpha \log \left| \frac{\Omega - 2}{\Omega + 2} \right|, \end{aligned}$$

$1 \leq \eta_\ell \leq 5$ is a dimensionless loss parameter (which we set to one), and the dimensionless constants Ω (scaled frequency), α (fine structure constant), and κ (scaled

chemical potential) are defined by

$$\Omega := \frac{\hbar\omega}{\mu}, \quad \alpha := \frac{e^2}{4\pi\epsilon_0\hbar c_0}, \quad \kappa := \frac{4k_B T}{\mu}.$$

In these

| | |
|--|----------------------------|
| $t = 2.7$ [eV] | hopping parameter, |
| $\hbar = 6.582119514 \times 10^{-16}$ [eV s] | reduced Planck's constant, |
| $k_B = 8.6173324 \times 10^{-5}$ [eV/K] | Boltzmann constant, |
| ω [rad/s] | angular frequency, |
| T [K] | temperature, |
| μ [eV] | chemical potential. |

From this the conductivity (measured in Siemens) is defined by

$$\sigma^{(g)} = \epsilon_0 c_0 \hat{\sigma}^{(g)},$$

where ϵ_0 is the permittivity of free space, and c_0 is the speed of light. In this work we view the temporal angular frequency (ω), temperature (T), and chemical potential (μ) as parameters to be varied, though we fix $T = 300$ K. Finally, we choose to measure lengths in microns and it is helpful to remember that for light of wavelength λ , the temporal angular frequency is given by $\omega = (2\pi c_0)/\lambda$ [rad/s].

B.1. The effective permittivity of graphene. To close, we formulate an “effective permittivity” for graphene based upon our model above which can be used in a nonvanishing layer approximation of a graphene layer. We recall that the complex permittivity of a layer is defined by

$$\epsilon := \epsilon' + i \frac{\Sigma}{\omega \epsilon_0},$$

where Σ is the conductivity in the bulk (measured in [S/m]). In [4, 2] they approximate this quantity by dividing σ by the thickness of the graphene layer, d_g , reported in [4] as 0.34 nm. With these considerations we define the effective permittivity of graphene by

$$\epsilon^{(g)} := \frac{i\sigma^{(g)}/d_g}{\omega \epsilon_0}.$$

Using the facts that $\omega = c_0 k_0$ and $\sigma^{(g)} = \epsilon_0 c_0 \hat{\sigma}^{(g)}$ we simplify this to

$$\epsilon^{(g)} = \frac{i\hat{\sigma}^{(g)}}{k_0 d_g}.$$

Appendix C. Vanishing thickness approximation of a finite graphene layer. In this section we consider an alternative derivation of the governing equations (3.7) and (3.8) by modeling the two-dimensional material as a layer with effective permittivity, $\epsilon^{(v)}$, of finite thickness, $d = d_g$, which we subsequently send to zero.

If the two-dimensional material occupies the domain

$$S^v = \{g(x) - d_g/2 < z < g(x) + d_g/2\},$$

we seek α -quasiperiodic solutions of

$$\begin{aligned}\Delta v + k_0^2 \epsilon^{(v)} v &= 0, & g(x) - d_g/2 < z < g(x) + d_g/2, \\ v(x, g(x) + d_g/2) &= V^u(x), \\ v(x, g(x) - d_g/2) &= V^\ell(x).\end{aligned}$$

Defining the outward pointing Neumann data

$$\tilde{V}^u(x) = (\partial_N v)(x, g(x) + d_g/2), \quad \tilde{V}^\ell(x) = -(\partial_N v)(x, g(x) - d_g/2),$$

and the DNO [45]

$$\begin{pmatrix} H & K \\ K & H \end{pmatrix} : \begin{pmatrix} V^u \\ V^\ell \end{pmatrix} \rightarrow \begin{pmatrix} \tilde{V}^u \\ \tilde{V}^\ell \end{pmatrix},$$

it is not difficult to write the governing equations in this scenario [45] as

$$\begin{aligned}U - V^u &= \zeta, \\ GU + \mu^2 HV^u + \mu^2 KV^\ell &= -\psi, \\ V^\ell - W &= 0, \\ KV^u + HV^\ell + \nu^2 JW &= 0,\end{aligned}$$

where

$$\mu^2 = \begin{cases} 1, & \text{TE,} \\ \epsilon^{(u)}/\epsilon^{(v)}, & \text{TM,} \end{cases} \quad \nu^2 = \begin{cases} 1, & \text{TE,} \\ \epsilon^{(v)}/\epsilon^{(w)}, & \text{TM.} \end{cases}$$

We have simplified by assuming continuity at the lower interface. Our goal is to write a system of two equations for $\{U, W\}$ by eliminating the appearance of $\{V^u, V^\ell\}$. To accomplish this we consider the final two equations above to give

$$\begin{aligned}V^\ell &= W, \\ V^u &= K^{-1} [-HV^\ell - \nu^2 JW] = -[K^{-1}H + \nu^2 K^{-1}J] W,\end{aligned}$$

where we used $V^\ell = W$ in the latter step. Inserting these into the first two equations above yields

$$\begin{aligned}U + K^{-1}HW + \nu^2 K^{-1}JW &= \zeta, \\ GU + \mu^2 H [-K^{-1}H - \nu^2 K^{-1}J] W + \mu^2 KW &= -\psi,\end{aligned}$$

or

$$(C.1) \quad \begin{pmatrix} I & (K^{-1}H + \nu^2 K^{-1}J) \\ G & \mu^2(K - HK^{-1}H) - \mu^2 \nu^2 HK^{-1}J \end{pmatrix} \begin{pmatrix} U \\ W \end{pmatrix} = \begin{pmatrix} \zeta \\ -\psi \end{pmatrix}.$$

We now study some of these operators in the flat-interface case and note that they are probably still true (essentially) for a sufficiently small deformation. To begin, we recall [45] that

$$\begin{aligned}H &= (i\gamma_D^{(v)}) \coth(i\gamma_D^{(v)} d_g) = (i\gamma_D^{(v)}) \left(\frac{1}{i\gamma_D^{(v)} d_g} + \dots \right) \sim \frac{1}{d_g} I, \\ K &= -(i\gamma_D) \operatorname{csch}(i\gamma_D^{(v)} d_g) = -(i\gamma_D^{(v)}) \left(\frac{1}{i\gamma_D^{(v)} d_g} + \dots \right) \sim -\frac{1}{d_g} I,\end{aligned}$$

so that

$$HK^{-1} = K^{-1}H = -\frac{1}{i\gamma_D^{(v)}} \sinh(i\gamma_D^{(v)}d_g)(i\gamma_D^{(v)}) \coth(i\gamma_D^{(v)}d_g) = -\cosh(i\gamma_D^{(v)}d_g) \sim -I,$$

$$K^{-1} = -\frac{1}{i\gamma_D^{(v)}} \sinh(i\gamma_D^{(v)}d_g) = -\frac{1}{i\gamma_D^{(v)}} \left(i\gamma_D^{(v)}d_g + \dots \right) \sim -d_g I,$$

while, using the identities

$$\operatorname{csch}^2 z - \coth^2 z = -1, \quad -(\gamma_p^{(v)})^2 = \alpha_p^2 - (k^{(v)})^2,$$

we have

$$\begin{aligned} K - HK^{-1}H &= K^{-1} (K^2 - KHK^{-1}H) \\ &= K^{-1} (K^2 - H^2) \\ &= K^{-1} (i\gamma_D^{(v)})^2 (-I) \\ &= -K^{-1} \left(-(\gamma_D^{(v)})^2 \right) \\ &= \frac{1}{i\gamma_D^{(v)}} \sinh(i\gamma_D^{(v)}d_g) \left\{ \alpha_D^2 - (k^{(v)})^2 \right\} \\ &= (d_g + \mathcal{O}(d_g^3)) \left\{ \alpha_D^2 - \epsilon^{(v)} k_0^2 \right\}. \end{aligned}$$

Using the relation $\epsilon^{(v)} = i\hat{\sigma}^{(g)}/(k_0 d_g)$ from Appendix B for the effective permittivity of the two-dimensional material, we find

$$\begin{aligned} K - HK^{-1}H &= (d_g + \mathcal{O}(d_g^3)) \left\{ \alpha_D^2 - \left(\frac{i\hat{\sigma}^{(g)}}{k_0 d_g} \right) k_0^2 \right\} \\ &= -i\hat{\sigma}^{(g)} k_0 + \mathcal{O}(d_g) \\ &= -\rho + \mathcal{O}(d_g). \end{aligned}$$

From this we learn that

$$\nu^2 K^{-1}J \sim \begin{cases} -d_g J \sim 0, & \text{TE,} \\ (-\eta/d_g)(-d_g J) = \eta J, & \text{TM,} \end{cases}$$

and

$$\mu^2 \nu^2 HK^{-1}J = -\tau^2 J = \begin{cases} -J, & \text{TE,} \\ -(\epsilon^{(u)}/\epsilon^{(w)})J, & \text{TM,} \end{cases}$$

and

$$\mu^2 (K - HK^{-1}H) \sim \begin{cases} -\rho, & \text{TE,} \\ 0, & \text{TM.} \end{cases}$$

Thus, in the TE configuration, as $d_g \rightarrow 0$, the governing equations (C.1) become

$$(C.2) \quad \begin{pmatrix} I & -I \\ G & J - \rho I \end{pmatrix} \begin{pmatrix} U \\ W \end{pmatrix} = \begin{pmatrix} \zeta \\ -\psi \end{pmatrix},$$

while in the TM configuration we have

$$(C.3) \quad \begin{pmatrix} I & -I + \eta J \\ G & \tau^2 J \end{pmatrix} \begin{pmatrix} U \\ W \end{pmatrix} = \begin{pmatrix} \zeta \\ -\psi \end{pmatrix}.$$

We point out that these match (3.7) and (3.8) exactly for $g \equiv 0$.

Acknowledgments. The author would like to thank Tony Low and Sang-Hyun Oh for extended conversations, helpful hints, and unwavering encouragement.

REFERENCES

- [1] *Graphene: Latest Research and Reviews*, <http://www.nature.com/subjects/graphene>, October 2016.
- [2] C. D. ANGELIS, A. LOCATELLI, A. MUTTI, AND A. ACEVES, *Coupling dynamics of 1d surface plasmon polaritons in hybrid graphene systems*, *Opt. Lett.*, 41 (2016), pp. 480–483.
- [3] T. ARENS, *Scattering by Biperiodic Layered Media: The Integral Equation Approach*, Habilitationsschrift, Karlsruhe Institute of Technology, Karlsruhe, Germany, 2009.
- [4] A. AUDITORE, C. DE ANGELIS, A. LOCATELLI, AND A. B. ACEVES, *Tuning of surface plasmon polaritons beat length in graphene directional couplers*, *Opt. Lett.*, 38 (2013), pp. 4228–4231.
- [5] G. A. BAKER, JR. AND P. GRAVES-MORRIS, *Padé Approximants*, 2nd ed., Cambridge University Press, Cambridge, UK, 1996.
- [6] G. BAO AND D. C. DOBSON, *Nonlinear optics in periodic diffractive structures*, in Second International Conference on Mathematical and Numerical Aspects of Wave Propagation (Newark, DE, 1993), SIAM, Philadelphia, 1993, pp. 30–38.
- [7] G. BAO, D. C. DOBSON, AND J. A. COX, *Mathematical studies in rigorous grating theory*, *J. Opt. Soc. Am. A*, 12 (1995), pp. 1029–1042.
- [8] C. M. BENDER AND S. A. ORSZAG, *Advanced Mathematical Methods for Scientists and Engineers*, International Series in Pure and Applied Mathematics, McGraw-Hill, New York, 1978.
- [9] Y. BLUDOV, A. FERREIRA, N. PERES, AND M. VASILEVSKIY, *A primer on surface plasmon-polaritons in graphene*, *Internat. J. Modern Phys. B*, 27 (2013), 1341001.
- [10] O. BRUNO AND F. REITICH, *Numerical solution of diffraction problems: A method of variation of boundaries*, *J. Opt. Soc. Am. A*, 10 (1993), pp. 1168–1175.
- [11] O. BRUNO AND F. REITICH, *Numerical solution of diffraction problems: A method of variation of boundaries II. Finitely conducting gratings, Padé approximants, and singularities*, *J. Opt. Soc. Am. A*, 10 (1993), pp. 2307–2316.
- [12] O. BRUNO AND F. REITICH, *Numerical solution of diffraction problems: A method of variation of boundaries. III. Doubly periodic gratings*, *J. Opt. Soc. Am. A*, 10 (1993), pp. 2551–2562.
- [13] O. R. BURGGRAF, *Analytical and numerical studies of the structure of steady separated flows*, *J. Fluid Mech.*, 24 (1966), pp. 113–151.
- [14] E. CARRASCO, M. TAMAGNONE, J. R. MOSIG, T. LOW, AND J. PERRUISSEAU-CARRIER, *Gate-controlled mid-infrared light bending with aperiodic graphene nanoribbons array*, *Nanotechnology*, 26 (2015), 134002.
- [15] J. CHANDEZON, D. MAYSTRE, AND G. RAOULT, *A new theoretical method for diffraction gratings and its numerical application*, *J. Opt.*, 11 (1980), pp. 235–241.
- [16] Y. CHEN, J. LIU, AND P. LIN, *Recent trend in graphene for optoelectronics*, *Journal of Nanoparticle Research*, 15 (2013), 1454.
- [17] D. C. DOBSON, *Optimal design of periodic antireflective structures for the Helmholtz equation*, *European J. Appl. Math.*, 4 (1993), pp. 321–339.
- [18] D. C. DOBSON, *A variational method for electromagnetic diffraction in biperiodic structures*, *RAIRO Modél. Math. Anal. Numér.*, 28 (1994), pp. 419–439.
- [19] S. ENOCH AND N. BONOD, *Plasmonics: From Basics to Advanced Topics*, Springer Series in Optical Sciences, Springer, New York, 2012.
- [20] D. FARMER, D. RODRIGO, T. LOW, AND P. AVOURIS, *Plasmon-plasmon hybridization and bandwidth enhancement in nanostructured graphene*, *Nano Letters*, 15 (2015), p. 2582.
- [21] B. FERGUSON AND X.-C. ZHANG, *Materials for terahertz science and technology*, *Nat. Mater.*, 1 (2002), pp. 26–33.
- [22] M. FUHRER, C. LAU, AND A. MACDONALD, *Graphene: Materially better carbon*, *MRS Bulletin*, 35 (2010), pp. 289–295.

- [23] A. GEIM, *Graphene: Status and prospects*, Science, 324 (2009), pp. 1530–1534.
- [24] A. GEIM, *Random walk to graphene (Nobel lecture)*, Angewandte Chemie International Edition, 50 (2011), pp. 6966–6985.
- [25] A. GEIM AND K. NOVOSELOV, *The rise of graphene*, Nature Materials, 6 (2007), pp. 183–191.
- [26] D. GIVOLI, *Recent advances in the DtN FE method*, Arch. Comput. Methods Engrg., 6 (1999), pp. 71–116.
- [27] H. D. HAN AND X. N. WU, *Approximation of infinite boundary condition and its application to finite element methods*, J. Comput. Math., 3 (1985), pp. 179–192.
- [28] Y. HE, M. MIN, AND D. P. NICHOLLS, *A spectral element method with transparent boundary condition for periodic layered media scattering*, J. Sci. Comput., 68 (2016), pp. 772–802.
- [29] Y. HE, D. P. NICHOLLS, AND J. SHEN, *An efficient and stable spectral method for electromagnetic scattering from a layered periodic structure*, J. Comput. Phys., 231 (2012), pp. 3007–3022.
- [30] B. HU AND D. P. NICHOLLS, *Analyticity of Dirichlet–Neumann operators on Hölder and Lipschitz domains*, SIAM J. Math. Anal., 37 (2005), pp. 302–320, <https://doi.org/10.1137/S0036141004444810>.
- [31] B. HU AND D. P. NICHOLLS, *The domain of analyticity of Dirichlet–Neumann operators*, Proc. Roy. Soc. Edinburgh Sect. A, 140 (2010), pp. 367–389.
- [32] J. B. KELLER AND D. GIVOLI, *Exact nonreflecting boundary conditions*, J. Comput. Phys., 82 (1989), pp. 172–192.
- [33] A. KUMAR, T. LOW, K. FUNG, P. AVOURIS, AND N. FANG, *Tunable light–matter interaction and the role of hyperbolicity in graphene-hbn system*, Nano Letters, 15 (2015), pp. 3172–3180.
- [34] T. LOW AND P. AVOURIS, *Graphene plasmonics for terahertz to mid–infrared applications*, ACS Nano, 8 (2014), pp. 1086–1101.
- [35] T. LOW, R. ROLDAN, W. HAN, F. XIA, P. AVOURIS, L. MORENO, AND F. GUINEA, *Plasmons and screening in monolayer and multilayer black phosphorus*, Phys. Rev. Lett., 113 (2014), 106802.
- [36] S. A. MAIER, *Plasmonics: Fundamentals and Applications*, Springer, New York, 2007.
- [37] A. MALCOLM AND D. P. NICHOLLS, *A field expansions method for scattering by periodic multilayered media*, J. Acoust. Soc. Am., 129 (2011), pp. 1783–1793.
- [38] A. MALCOLM AND D. P. NICHOLLS, *Operator expansions and constrained quadratic optimization for interface reconstruction: Impenetrable acoustic media*, Wave Motion, 51 (2014), pp. 23–40.
- [39] D. M. MILDER, *An improved formalism for rough-surface scattering of acoustic and electromagnetic waves*, in Proceedings of SPIE – The International Society for Optical Engineering, Vol. 1558, (San Diego, 1991), Int. Soc. for Optical Engineering, Bellingham, WA, 1991, pp. 213–221.
- [40] D. M. MILDER, *An improved formalism for wave scattering from rough surfaces*, J. Acoust. Soc. Am., 89 (1991), pp. 529–541.
- [41] D. M. MILDER AND H. T. SHARP, *Efficient computation of rough surface scattering*, in Mathematical and Numerical Aspects of Wave Propagation Phenomena (Strasbourg, 1991), SIAM, Philadelphia, 1991, pp. 314–322.
- [42] D. M. MILDER AND H. T. SHARP, *An improved formalism for rough surface scattering. II: Numerical trials in three dimensions*, J. Acoust. Soc. Am., 91 (1992), pp. 2620–2626.
- [43] D. P. NICHOLLS, *A rapid boundary perturbation algorithm for scattering by families of rough surfaces*, J. Comput. Phys., 228 (2009), pp. 3405–3420.
- [44] D. P. NICHOLLS, *Efficient enforcement of far-field boundary conditions in the transformed field expansions method*, J. Comput. Phys., 230 (2011), pp. 8290–8303.
- [45] D. P. NICHOLLS, *Three-dimensional acoustic scattering by layered media: A novel surface formulation with operator expansions implementation*, Proc. R. Soc. Lond. Ser. A Math. Phys. Eng. Sci., 468 (2012), pp. 731–758.
- [46] D. P. NICHOLLS, *A method of field expansions for vector electromagnetic scattering by layered periodic crossed gratings*, J. Opt. Soc. Am. A, 32 (2015), pp. 701–709.
- [47] D. P. NICHOLLS, *Numerical solution of diffraction problems: A high-order perturbation of surfaces and asymptotic waveform evaluation method*, SIAM J. Numer. Anal., 55 (2017), pp. 144–167, <https://doi.org/10.1137/16M1059679>.
- [48] D. P. NICHOLLS AND N. NIGAM, *Exact non-reflecting boundary conditions on general domains*, J. Comput. Phys., 194 (2004), pp. 278–303.

- [49] D. P. NICHOLLS, S.-H. OH, T. W. JOHNSON, AND F. REITICH, *Launching surface plasmon waves via vanishingly small periodic gratings*, J. Opt. Soc. Am. A, 33 (2016), pp. 276–285.
- [50] D. P. NICHOLLS AND J. ORVILLE, *A boundary perturbation method for electromagnetic scattering from families of doubly periodic gratings*, J. Sci. Comput., 45 (2010), pp. 471–486.
- [51] D. P. NICHOLLS AND F. REITICH, *A new approach to analyticity of Dirichlet-Neumann operators*, Proc. Roy. Soc. Edinburgh Sect. A, 131 (2001), pp. 1411–1433.
- [52] D. P. NICHOLLS AND F. REITICH, *Stability of high-order perturbative methods for the computation of Dirichlet-Neumann operators*, J. Comput. Phys., 170 (2001), pp. 276–298.
- [53] D. P. NICHOLLS AND F. REITICH, *Analytic continuation of Dirichlet-Neumann operators*, Numer. Math., 94 (2003), pp. 107–146.
- [54] D. P. NICHOLLS AND F. REITICH, *Shape deformations in rough surface scattering: Cancellations, conditioning, and convergence*, J. Opt. Soc. Am. A, 21 (2004), pp. 590–605.
- [55] D. P. NICHOLLS AND F. REITICH, *Shape deformations in rough surface scattering: Improved algorithms*, J. Opt. Soc. Am. A, 21 (2004), pp. 606–621.
- [56] D. P. NICHOLLS AND F. REITICH, *Boundary perturbation methods for high-frequency acoustic scattering: Shallow periodic gratings*, J. Acoust. Soc. Am., 123 (2008), pp. 2531–2541.
- [57] D. P. NICHOLLS, F. REITICH, T. W. JOHNSON, AND S.-H. OH, *Fast high-order perturbation of surfaces (HOPS) methods for simulation of multi-layer plasmonic devices and metamaterials*, J. Opt. Soc. Am. A, 31 (2014), pp. 1820–1831.
- [58] K. NOVOSELOV, *Graphene: Materials in the flatland (nobel lecture)*, Angewandte Chemie International Edition, 50 (2011), pp. 6986–7002.
- [59] K. S. NOVOSELOV, A. K. GEIM, S. V. MOROZOV, D. JIANG, Y. ZHANG, S. V. DUBONOS, I. V. GRIGORIEVA, AND A. A. FIRSOV, *Electric field effect in atomically thin carbon films*, Science, 306 (2004), pp. 666–669.
- [60] R. PETIT, ed., *Electromagnetic Theory of Gratings*, Springer-Verlag, Berlin, 1980.
- [61] N. A. PHILLIPS, *A coordinate system having some special advantages for numerical forecasting*, J. Atmospheric Sci., 14 (1957), pp. 184–185.
- [62] H. RAETHER, *Surface Plasmons on Smooth and Rough Surfaces and on Gratings*, Springer, Berlin, 1988.
- [63] P. J. ROACHE, *Code verification by the method of manufactured solutions*, J. Fluids Eng., 124 (2002), pp. 4–10.
- [64] D. RODRIGO, T. LOW, D. FARMER, H. ALTUG, AND P. AVOURIS, *Plasmon coupling in extended structures: Graphene superlattice nanoribbon arrays*, Phys. Rev. B, 93 (2016), 125407.
- [65] C. J. ROY, *Review of code and solution verification procedures for computational simulation*, J. Comput. Phys., 205 (2005), pp. 131–156.
- [66] R. SOREF, *Mid-infrared photonics in silicon and germanium*, Nat. Photonics, 4 (2010), pp. 495–497.
- [67] T. STAUBER, N. M. R. PERES, AND A. H. CASTRO NETO, *Conductivity of suspended and non-suspended graphene at finite gate voltage*, Phys. Rev. B, 78 (2008), 085418.
- [68] M. TONOUCHI, *Cutting-edge terahertz technology*, Nat. Photonics, 1 (2007), pp. 97–105.
- [69] J. WILKENING AND V. VASAN, *Comparison of five methods of computing the Dirichlet-Neumann operator for the water wave problem*, in Nonlinear Wave Equations: Analytic and Computational Techniques, Contemp. Math. 635, AMS, Providence, RI, 2015, pp. 175–210.
- [70] H. YAN, T. LOW, F. GUINEA, F. XIA, AND P. AVOURIS, *Tunable phonon-induced transparency in bilayer graphene nanoribbons*, Nano Letters, 14 (2014), pp. 4581–4586.
- [71] P. YEH, *Optical Waves in Layered Media*, Wiley Series in Pure and Applied Optics 61, Wiley-Interscience, Hoboken, NJ, 2005.